A study on the numerical prediction of cavitation erosion for propellers

Onur Usta[1]*, Batuhan Aktas[2], Matthias Maasch[2], Osman Turan[2], Mehmet Atlar[2], Emin Korkut[1]

[1]Faculty of Naval Architecture and Ocean Engineering, Istanbul Technical University, Istanbul, Turkey
[2]Department of Naval Architecture, Ocean and Marine Engineering, University of Strathclyde, Glasgow, UK

ABSTRACT

This paper presents a numerical study on the prediction of performance, cavitation and erosion characteristics of King's College-D (KCD)-193 model propeller in different flow conditions. The present work is achieved by using unsteady Detached Eddy Simulation (DES) turbulence model in a Computational Fluid Dynamics (CFD) software STAR-CCM+. Cavitation is modelled by Schnerr-Sauer cavitation model with Reboud correction. Flow velocity and flow turbulent intensity, derived from Laser Doppler Anemometry (LDA) measurements conducted at the Emerson Cavitation Tunnel for the KCD-193 propeller, are applied as numerical boundary fields for the inlet of the cavitation tunnel domain to reflect the experimental flow conditions. Cavitation erosion is modelled by three different approaches using pressure, saturation pressure, volume fraction of vapour, time derivative of the pressure and time derivative of the volume fraction of vapour on the propeller blades obtained from simulations. A new approach to predict cavitation erosion intensity on the propeller blade is proposed. The preliminary results of the study are compared with the experimental results carried out at Emerson Cavitation Tunnel of Newcastle University. Qualitative cavitation extent and erosion comparisons are made for different conditions. Computation results are in good agreement with those of experiments.

Keywords
Propeller, DES, multi-phase flows, cavitation modelling, cavitation erosion

1 INTRODUCTION

Cavitation is a complex fluid mechanics phenomenon for nozzles, pumps, injectors, turbines, propellers and a variety of other fluid machinery components and the occurrence of cavitation is often inevitable for hydro machinery. It causes undesired effects such as noise, vibration, power loss and erosion. The last phenomenon, cavitation erosion is perhaps the most remarkable damaging consequence of cavitation and can severely damage propeller by removing material from the surface (Tseng 2010; Jian et al 2015).

Prediction of the cavitation erosion is a complex phenomenon since it includes both hydrodynamic and material science knowledge (Franc & Michel, 2004). Due to the nonlinear nature of their dynamics, the governing equations are not fully solvable, which requires extensive effort to fully understand and accurately predict (Eskilsson & Bensow, 2015).

In order to numerically predict cavitation erosion, it is necessary to accurately model the cavitating flow and correlate the flow features to erosion damages. Despite numerous research efforts, cavitation erosion is not yet well understood and it is subject of ongoing research studies. (Li 2012; Koukouvinis et al, 2015; Eskilsson & Bensow 2015; Bergeles et al 2015). The studies below are some of the important steps of cavitation erosion modelling using CFD in literature.

Nohmi et al (2008) and Hasuike et al (2009) developed four erosive function indices which are based on pressure and volume fraction time derivatives as well as absolute pressure difference. Dular & Delgosha (2009), investigated the possibility of predicting cavitation erosion for hydrofoils using CFD. Their CFD model was based on the numerical solution of the unsteady Reynolds-Averaged Navier-Stokes (RANS) equations coupled with a homogeneous equilibrium barotropic model.

Terwisga et al (2009), revised some cavitation erosion models. In those models, the potential energy of the bubble, *Ep*, is described as the main erosion factor when a group of bubbles collapse simultaneously in cascade and the gap between the wall and the cloud of bubbles is very thin. They presented a post-processing procedure for the assessment of the cavitation erosion risk based on multiphase CFD results on the experimental observations. They made a correlation between the available information that came from multiphase RANS and the experimental observations obtained by a high-speed video.

Bensow & Bark (2010), investigated the sheet cavitation on a ship propeller by both experimentally and numerically. It is noted that the sheet cavity seems to induce more severe erosion damage than the large cloud cavity, which implies that the micro cavity collapses are the main reason contributing to the damage.

Lloyd's Register has performed cavitation observations and measurements at ship scale and Lloyd's Register Technical Investigation Department (LR TID) has developed its own erosive functions which were

reported in Boorsma & Whitworth (2011). These observations showed that details of the cavitating flow are paramount for the erosive potential of the flow. Ochiai et al (2012), proposed a simulation method for predicting the cavitating flow around a NACA0015 hydrofoil. The impact pressures on the solid surface were analysed. They made a quantitative numerical prediction of cavitation erosion in a cavitating flow.

Li (2012), proposed an erosion intensity function for the assessment of the risk of cavitation erosion on the hydrofoil surface by post-processing the results predicted by a multiphase RANS method. In that study, the qualitative correlation between the risk of cavitation erosion and unsteady cavitation phenomena has been investigated by post processing the unsteady RANS results of a NACA0015 hydrofoil and an NACA0018-45 hydrofoil. Among the several criteria suggested by Li (2012), the time derivative of the local pressure $\partial p/\partial t$ shows the best correlation with the observed damaged areas. A new erosion intensity function is then presented based on the mean of $\partial p/\partial t$ values that exceed a certain threshold. Eskilsson and Bensow (2015), looked into three different approaches for obtaining estimates of the potential cavitation erosion intensity from CFD simulations. Two of the methods that they applied were using the pressure or the vapour fraction obtained from macroscopic simulation and one based on the pressure obtained from microscopic bubble dynamics. The three methods were applied to the case of cavitating flow over a NACA0015 foil. None of the methods was found to successfully predict the erosive behaviour.

Hidalgo et al (2015) studied numerical simulation of erosive partial cavitation around a NACA0015 hydrofoil. They calculated the bubble collapse strength based on the potential energy and homogeneous mixture flow assumption using implicit Large Eddy Simulation (LES) and Zwart-Gerber-Belamri cavitation model (Zwart et al 2004).

Jian et al (2015), compared results of the numerical simulations against high-speed simultaneous observations of cavitation and cavitation erosion. Good agreements were noticed between calculations and experiments. Two high-pressure peaks were found during one cavitation cycle. One relates to the cavitation collapse and the other one corresponds to the cavitation shed off, both contributing to a distinctive stepwise erosion damage growth pattern. Koukouvinis et al (2015) proposed a methodology for predicting the region of bubble collapse and its cavitation aggressiveness. The idea for the proposed methodology is based on the concept that for a vapour bubble to collapse two conditions should be met: (1) the total derivative of the vapour volume fraction should be negative (as bubbles should have decreasing volume) or equally the total derivative of the mixture density should be positive and (2) the total derivative of the pressure should be positive (bubbles collapse at regions of increasing pressure). Bergeles et al (2015) presented an Erosion Aggressiveness Index (EAI) based on the pressure loads which develop on the material surface and the material yield stress. The predicted surface area prone to the cavitation damage is compared with the experiments. The EAI predictions indicate the minimum bubble size above the which erosion starts as also its location along the injector wall. Ponkratov and Caldas (2015) developed a method for numerical erosion prediction which is effective across a range of Reynolds numbers for both model scale and full scale. They carried out a CFD simulation of the containership in full scale under the condition recorded during the tests. At the end of the study, new erosion functions have been developed for the propeller and rudder and validated against those in model and ship scale.

Within this context various numerical cavitation models have been introduced in the literature and numerous cavitating flow simulations were conducted using CFD. However, the cavitation modelling is still very challenging since it involves the interactions between the two phases, liquid and vapour, and moreover rapid temporal and spatial variations of the flow properties. (Benjamin & Ellis 1996; Li 2012; Vallier 2013; Ponkratov & Caldas 2015).

Numerical methods can be broadly categorized into Reynolds-Averaged Navier–Stokes (RANS), Detached Eddy Simulation (DES), Large Eddy Simulation (LES) and Direct Numerical Simulation (DNS). While the RANS simulations use equations which give good estimations of the turbulent flow physics, LES and DNS resolve the governing equations and thus give more insight into the flow details (Bensow & Bark, 2010, Maasch et al 2015).

The RANS model is widely used in the calculations of turbulent cavitating flows. In this turbulence model, the averaged quantities are obtained, ignoring the small-scale turbulence structure. The method of a higher resolution can better help to study the influence of pressure fluctuations on the cavitating flow (Zhang et al, 2015). The DES combines the RANS method with the LES method where the RANS gives solutions in a reasonable period of time by modelling the attached turbulent flow near the geometry wall, whilst the LES method, actually solves the free flow physics (Maasch et al 2015). The LES is based on computing the large, energy-containing structures that are resolved on the computational grid, whereas the smaller, more isotropic, sub-grid structures are modelled. To benefit from the advantages of LES and DNS the numerical grid must be fine and also the time step of the computation has to be kept very small. These requirements have a major impact on the necessary computational time. The study of Muscari et al (2012), reports that although the DNS approach is available, the use of this method is very difficult for time-critical industrial applications, due to the requirement of very high computational times (Maasch et al 2015).

The DES seems to be a good alternative to keep the computational time in a reasonable frame but also to

solve the flow structures as detailed as necessary (Maasch et al 2015). Muscari et al (2012) showed that the DES solves physics on a smaller scale and thus makes the results more reliable, compared to the RANS simulations. Moreover, Zhang et al (2015) also indicated that the DES is a feasible turbulence model for the simulation of the tip vortex cavitating flows.

Considering the advantages, cavitating flow is modelled with the DES turbulence model in order to solve the flow structures as detailed as necessary and keep the computational time in an applicable frame in the study. STAR-CCM+ is used as flow solver.

In the study, two erosion indicators presented in the literature are applied to predict erosion regions on the propeller:

i) The Intensity Function Method (IFM), which uses the time derivative of the pressure to correlate the erosion intensity (Li and Terwisga, 2012).

ii) The *Gray Level Method* (GLM), which relates the standard deviation of vapour fraction to the erosive energy (Dular et al 2006).

After that, a new erosive indicator is proposed combining these two methods:

iii) The Erosive Power Method (EPM), which focus on both the derivative of the vapour fraction and the derivative of pressure.

The name of the new proposed method is taken from Eskilsson & Bensow (2015). However, it is used as an erosive indicator, for the first time, in this paper in the literature. These methods are still in development and require extensive research efforts before being useful and reliable. The present paper is a contribution to this subject. It adds a new point of view and presents a combined method of prediction of the erosion intensity applicable to CFD analysis.

Main objectives of the study are try to model cavitating flow and make accurate predictions of KCD-193 propeller performance. It is also aimed to obtain fairly good erosion distribution on the same propeller. CFD results of the KCD-193 propeller in two different conditions are compared with the experimental data carried out at the Emerson Cavitation Tunnel (ECT) of Newcastle University.

Within the above context this paper presents the prediction of hydrodynamic characteristics and erosion distribution on KCD-193 model propeller in particular cavitating flow conditions. Section 2 gives the description of experimental set-up and test conditions. Section 3 presents the details of CFD methodology. Section 4 includes the cavitation erosion modelling. Section 5 presents the results and discussions and finally Section 6 draws conclusions from the study.

2 DESCRIPTION OF EXPERIMENTAL SET- UP AND TEST CONDITIONS

The cavitating flow experiments were performed at Emerson Cavitation Tunnel (ECT) of Newcastle University (Mantzaris et al 2015). This tunnel is a vertical plane, closed circulating design and capable of reaching flow speeds up to 8 m/s. The tunnel is shown in Figure 1. Further details of ECT can be found in (Atlar, 2011).

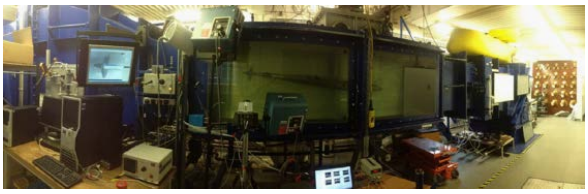

Figure 1: A panoramic view of Emerson Cavitation Tunnel

2.1 Cavitation tunnel set up

Propeller flow, when the propeller operating behind the hull, is affected by the presence of the ship's hull. During model scale cavitation testing inside the tunnel, the role of the hull may be replaced by the presence of 2D wake screens for practical and cost economical means (Mantzaris et al 2015).

In this study, an available 2D wake screen, which was called "ECT-W1" (Aktas et al 2015; Mantzaris et al 2015) was used to simulate the wake effect. Using the standard procedure in ECT this wake screen, which is a 500mm x 500mm (B x H) steel frame with varying size of wire meshes, was placed upstream of the propeller at a distance of approximately 1.5 times the model propeller diameter of 0.3048m. The wake survey was carried out by a LDA system (Aktas et al 2015). Figure 2 shows this wake arrangement inside the cavitation tunnel and Figure 3 shows its axial velocity ratio distribution, i.e. (1-w).

Figure 2: ECT-W1wake screen inside ECT (Aktas et al 2015; Mantzaris et al 2015)

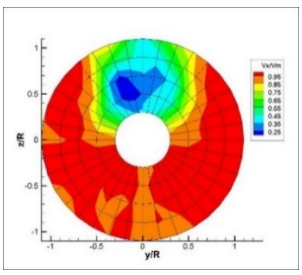

Figure 3: Axial velocity ratio distribution (ECT W1 representation-2D contour plot), (Aktas et al 2015; Mantzaris et al 2015)

Figure 4 shows model of the cavitation tunnel set-up.

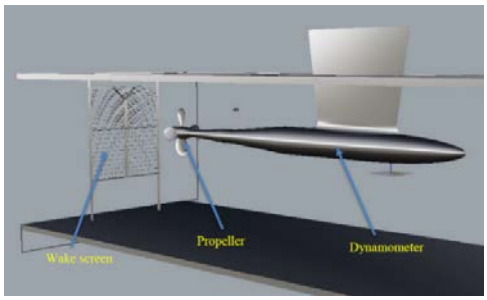

Figure 4: Model of the experimental set-up (Aktas et al 2015)

Plexiglass windows of the tunnel covering entire measuring section allowed a clear view of the propeller blades. Different optical media were used for the observation of the overall extend of cavitation phenomenon as well as the constant monitoring of the coating condition. A high-speed camera for video recording was mounted externally near the fiberglass window, alongside with a digital single-lens reflex (SLR) camera. This camera system had only manual pan and tilt capability, but their position was allowing view to sweep radially and tangentially relative to the propeller. A stroboscopic light system was set up to trigger off of a one-pulse per revolution signal, syncing the 6 strobe flashes with the propeller rotation. Some frames were lit by the strobe and some were dark using this lighting scheme with the camera. The dark frames were removed to obtain some continuous frame sequences with the propeller motion "frozen" by the strobe light (Mantzaris et al 2015). Figure 5 shows the monitoring as well as imaging and lighting set-up.

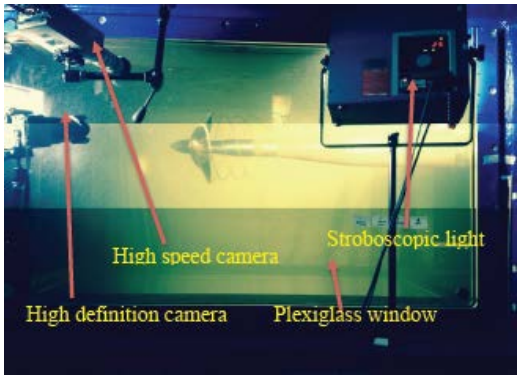

Figure 5: Monitoring and lighting set-up at measuring section of ECT (Mantzaris et al 2015)

In order to detect the blade area where cavitation erosion would occur, the blades of the propeller were coated with stencil inks, acrylic paints and engineering blue. The area where the ink was removed gave an indication where erosion damage would occur after extended operation.

Experiments were carried out with King's College-D (KCD)-193 propeller. KCD series model propellers originally included a series of model propellers, for which interesting full-scale results were available and the purpose of the series was to try and correlate the observed phenomena in the tunnel with the results of particular experience on ships. The characteristics of KCD-193 propeller is given in Table 1.

Table 1: KCD-193 propeller characteristics

Propeller diameter, D	0.3048 m
$BAR=A_E/A_0$	0.65
P/D	1
Number of blades, Z	4
Direction of rotation	Right handed
Material	Manganese Bronze

For the tunnel tests and CFD simulations, calculations were carried out using the following key parameters for each condition.

The cavitation number, based on rotational speed of the propeller is defined as

$$\sigma_n = \frac{P_{ref} - P_v}{0.5\rho\,(nD)^2} \qquad (1)$$

where P_{ref} is the reference pressure (P_A + $\rho g h_s$), (atmospheric pressure + hydrostatic pressure), P_v is the vapour pressure, ρ is the density of water, n is propeller rate of rotation and D is the diameter of the propeller and h_s is the propeller shaft immersion.

The advance coefficient is defined as

$$J = \frac{V_A}{n\,D} \qquad (2)$$

where V_A is the advance velocity and thrust and torque coefficient of the propeller are calculated as

$$K_T = \frac{T}{\rho\, n^2\, D^4}, \qquad K_Q = \frac{Q}{\rho\, n^2\, D^5} \qquad (3)$$

where T and Q are thrust and torque values of the propeller, respectively.

Open water efficiency of the propeller is defined as

$$\eta_0 = \frac{J}{2\pi}\frac{K_T}{K_Q} \qquad (4)$$

Experimental conditions are given in Table 2.

Table 2: Experimental conditions

	P_{ref} (kPa)	n (rps)	V_A (m/s)	J	σ_n
case 1 (Atmospheric condition)	117.011	25	3	0.393	3.88
case 2 (Vacuum condition)	77.016	25	3	0.392	2.52

The tests were composed of erosion and performance measurements of the propeller behind the wake screen under two different cavitating flow conditions. The first experiment (case 1) was performed at the atmospheric condition while the second experiment (case 2) was performed under vacuum condition.

The rotational speed of the propeller and inflow speed of the tunnel were kept constant for the cavitation experiments used in this study.

3 CFD METHODOLOGY

This section of the study contains cavitating flow simulations of KCD-193 propeller in 2 different cavitation conditions using DES turbulence model. After predicting cavitation characteristics, cavitation erosion on the propeller blades is predicted numerically using 3 different methods, which are given in section 4. The results of the simulations are compared with the experiments which were carried out at Emerson Cavitation Tunnel (ECT) of Newcastle University for wake flow and uniform flow conditions in 2015.

3.1 Computational Domain

The computational (numerical) domain is generated as the same dimensions as ECT except for the length of the outlet. The propeller is located 0.4572 m (the same as in the experiments) away from the inlet, 3m away from the outlet. The computational domain is shown in Figure 6.

Figure 6: Computational domain

The numerical domain consists of a static domain representing the cavitation tunnel and a rotational domain around the propeller employing a sliding mesh approach. The domain boundaries are defined as velocity inlet and pressure outlet. The tunnel wall and the propeller are defined as wall type.

The numerical mesh is a structured grid, and basic cells are tetrahedral and prismatic cells are applied to near the blade surface for resolving the boundary layer. Figure 7 shows grid over the rotational domain.

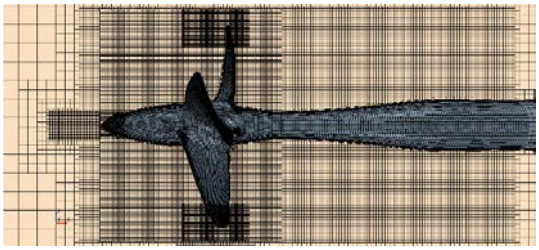

Figure 7: Grid over the rotational domain

Local volume refinements around the blade tips and propeller hub were carried out, in order to capture the cavitation extent with high resolution. The grid on the propeller surface Figures 8 and 9 below.

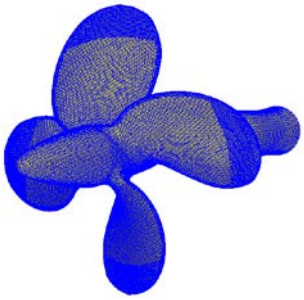

Figure 8: Grid on the propeller surface

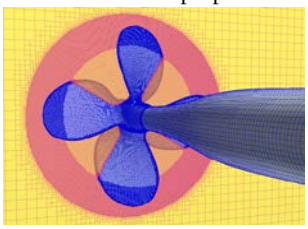

Figure 9: Grid over the propeller

In order to accurately model the interaction between the phases and to capture the cavitation interface in the solution domain, the numerical mesh resolution should be sufficiently fine (Maasch 2015). To achieve the best mesh resolution, a grid independence study was performed and the mesh was refined step by step until satisfactory solutions were obtained. In addition the turbulence length ratio in the bulk mesh was plotted as suggested by Maasch et al. This mesh test showed that a mesh of 24 million cells would needed to be further refined by a factor of approximately 40 in each spatial direction to solve even the smallest scales of turbulence. It was not attempted to reach such a high resolution as this would require very high computational power. The resulting mesh for the DES simulation was approximately 24 million cells; 21 million of which were in the rotating mesh region.

3.2 Cavitating Flow Analysis

To simulate cavitating flows, the two phases, liquid and vapour, need to be represented in the problem, as well as the phase transition mechanism between the two (Bensow & Bark 2010).

DES model with Shear Stress Transport (SST) Mentor k-omega Detached Eddy is used to model turbulent flow. Two phases, water and vapour are described by the equation of volume of fraction of vapour. The phases are mixed respect to their length scales using Eulerian multiphase model. Multiphase is modelled with Volume of Fluid (VOF). The VOF model assumes that the fluid is homogenous so that both phases share the same properties, such as velocity and pressure.

Figure 10 shows the frequency of the *Wall-*Y^+ on the propeller blade cells to be mostly under $Y^+ \leq 2$ which indicates that the viscous sublayer is well resolved. For regions holding a higher Y^+value wall functions are applied.

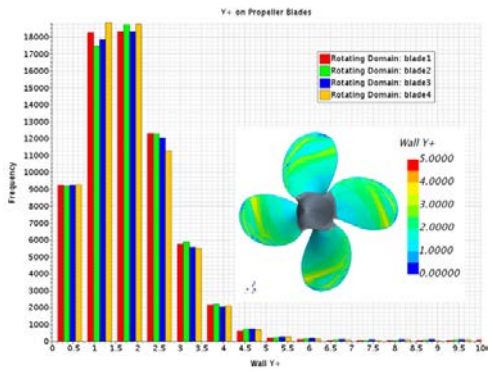

Figure 10: Frequency of the *Wall*-Y+ on the propeller blade cells

In order to capture the unsteady phenomena of cavitating flow, a step of $\Delta t = 2 * 10^{-5} s$ was chosen. This provided a very small rotation angle of $\Delta\alpha = 0.18°$ within one time step and a sufficient Convective Courant Number (CFL), which control the size of the local time step, on the VOF interface (see Figure 11 below).

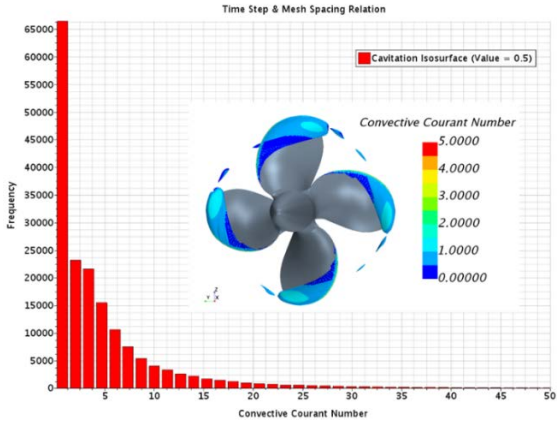

Figure 11: Convective Courant number on the cavitation isosurface

Figure 11 shows that the Convective Courant number on the cavitation isosurface (iso value 0.5) is mostly around CFL=1.

Cavitation is modelled by Schnerr-Sauer cavitation model with Reboud correction (Reboud et al 1998). Schnerr-Sauer cavitation model implements a reduced Rayleigh-Plesset equation and which neglects the influence of bubble growth acceleration, viscous effects, and surface tension effects. Mathematical background of the model was published in 2001. (Schnerr & Sauer 2001). In multiphase material properties part, seed density and seed diameter are defined the same as those in the ECT experiments. Assuming that the bubble is spherical and the bubble growth is an inertial-controlled process, the Rayleigh–Plesset equation is used to account for time evolution rate of the bubble radius. The Rayleigh-Plesset equation is an approximation that is derived for idealized conditions.

CFD conditions are generated as the same as experiments. Velocity and turbulence intensity are given as field functions according to LDV measurements.

Figure 12 shows velocity distribution of CFD analysis in the inlet.

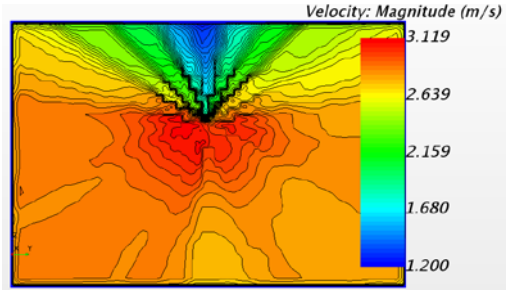

Figure 12: Velocity distribution of CFD analysis in inlet conditions

4 CAVITATION EROSION MODELING

In this part of the study, three different erosion indicators presented in the literature are reviewed: The Intensity Function Method (IFM), The Gray Level Method (GLM) and The Discrete Bubble Method (DBM). Afterward new proposed Erosive Power Method (EPM) which is a combination of GLM and IFM is explained.

These methods do not consider the material-related aspects of the cavitation-erosion process. But they aim to provide a qualitative or relative quantitative estimation of the erosive potential of the cavitating flow (Ponkratov & Caldas 2015).

4.1 Intensity Function Method (IFM)

This method uses the time derivative of the pressure to correlate the erosion intensity. In this paper, it is based on the values of the time derivative of the local pressure that exceeds two certain thresholds. Cavitation erosion on the propeller surface is limited by thresholds that show maximum and minimum value of the time derivative of the local pressure. Specifying the user-given threshold on cavitation erosion predictions for the predictions are done using ECT experimental data.

Li and Van Terwisga (2012) defined the erosion indicator of the IFM as;

$$I_{IFM} = \frac{1}{N}\sum Ii, \qquad Ii = \begin{cases} \frac{\partial P}{\partial t}, & if\ \frac{\partial P}{\partial t} > \in \\ 0, & otherwise \end{cases} \qquad (5)$$

It is indicated by the above Eq. (5) that a proper prediction of the cavitation erosion risk depends on the instantaneous local pressure gradient at each time step. Application of this equation results in a spatial distribution of the intensity function over the material surface.

A series of thresholds are applied to Eq. (5) to accurately evaluate the erosion intensity on the propeller surfaces. It is found that when the threshold level is applied between the values of $1*10^{-7}$ and $-1*10^{-7}$ and between the values of 0 and $-1*10^{-7}$ the erosion damage illustrations are very similar to the scenes obtained from ECT experimental study.

4.2 Gray Level Method (GLM)

This method is first suggested by Dular et al (2006) and the idea of it is to relate the standard deviation of vapour fraction to the erosive energy (Eskilsson & Bensow 2015).

The GLM is a direct numerical technique used to relate experimental data to erosion. The basis behind the GLM is that the power of the acoustic pressure wave is proportional to the pressure difference between the vapour pressure and the surrounding pressure in the liquid and the rate of change in vapour volume:

$$P_{pot} = (P - P_v)\left(\frac{dV_v}{dt}\right) \quad (6)$$

Where P_{ref} is reference pressure, P_v is saturation pressure and $\frac{dV_v}{dt}$ is time derivative of volume fraction of vapour on the propeller blades.

The equation (6) is directly calculated and applied to our flow solver by writing a field function to estimate the erosion indicator on the propeller surface.

4.3 Discrete Bubble Method (DBM)

The DBM is fundamentally different from the other two cavitation erosion indicators in that the DBM is based on the development of advected microscopic bubbles (Eskilsson and Bensow, 2015). In that method, the erosive intensity is estimated by computed the pressure inside the advected microscopic bubbles using Rayleigh Plesset equation (Eskilsson and Bensow, 2015).

4..4 New proposed Erosive Power Method (EPM)

Erosive power method is a combination of GLM and IFM. It is based on reference pressure, saturation pressure, volume fraction of vapour, time derivative of the pressure and volume fraction of vapour on the propeller blades.

It is defined mathematically as:

$$I_{EPM} = (P - P_v)\left(\frac{dV_v}{dt}\right) + V_V\left(\frac{dP}{dt}\right) \quad (7)$$

The methods GLM and IFM are based on Eq. 7 also. However, they focus on the different terms. The GLM focus on the derivative on the vapour fraction, while the IFM is based on the derivative of pressure (Eskilsson & Bensow 2015). New proposed erosive power method focusses on both derivatives of pressure and vapour fraction.

In this study, the DBM method was not used due to the requirement of very high computational power. Therefore new proposed EPM, the GLM and the IFM were used in the analysis.

5 RESULTS AND DISCUSSIONS

5.1 Comparison of Cavitating Flow Analysis Results

The comparison of the experimental and CFD results for cavitating flow analysis is given in this section.

Figure 13 shows the propagation of cavitation on KCD-193 for case 1 condition and Figure 14 shows CFD analysis under the condition corresponding to picture 8 in Figure 13. The iso-contour is taken as 0.5 in the analysis.

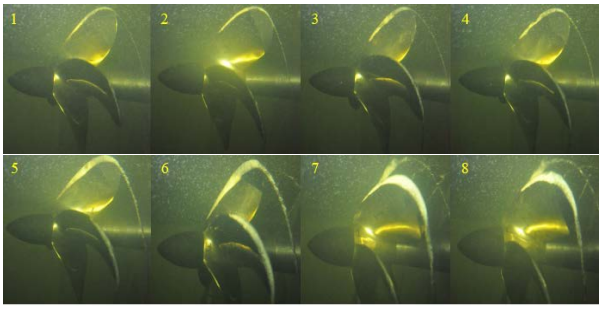

Figure 13: Cavitation observations with KCD-193 at atmospheric condition (case 1)

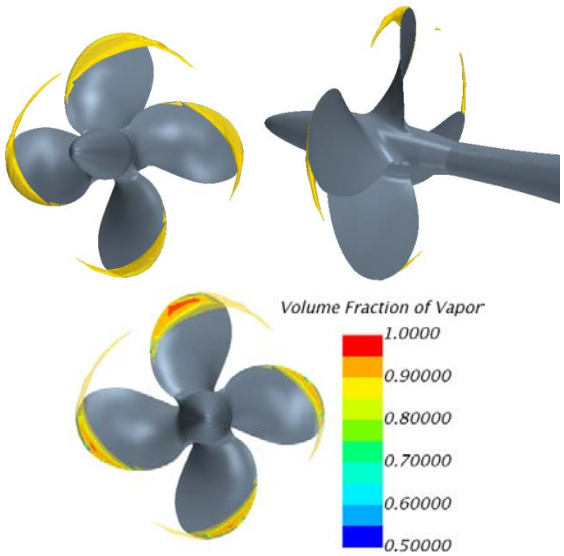

Figure 14: Volume fraction of vapour of KCD-193 at atmospheric condition (case 1)

Figure 15 shows the propagation of cavitation on KCD-193 for case 2 condition and Figure 16 shows CFD analysis under the condition corresponding to picture 8 in Figure 15. The iso-contour is taken as 0.5 in the analysis.

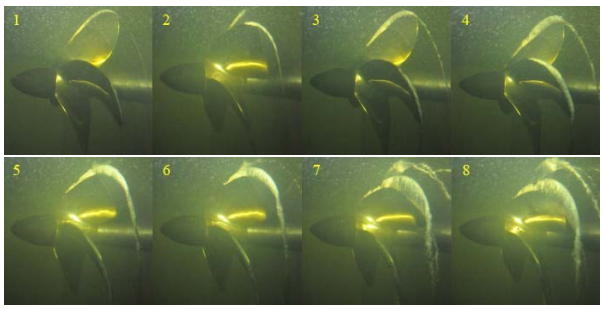

Figure 15: Cavitation observations with KCD-193 at vacuum condition (case 2)

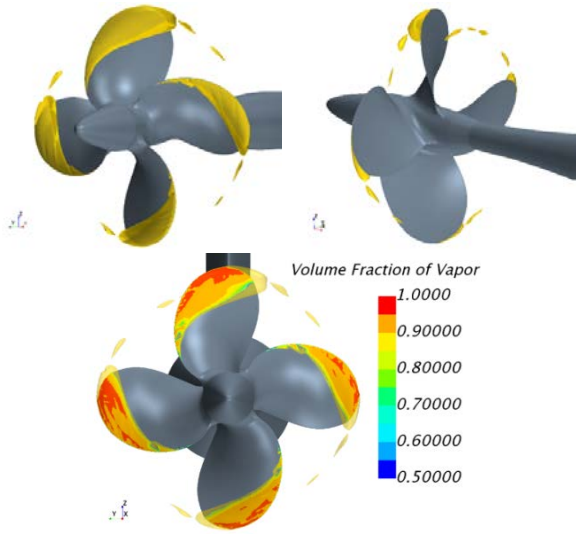

Figure 16: Volume fraction of vapour of KCD-193 at vacuum condition (case 2)

The comparison of the cavitation extent by the numerical analysis and that of experiment shows a good agreement as can be seen from the figures above. On the other hand the tip vortex trail is not predicted completely due to the insufficient mesh resolution downstream of the propeller.

The performance of propeller is conventionally represented in terms of non-dimensional coefficients, i.e., thrust coefficient (K_T), torque coefficient (K_Q) and open water efficiency (η_0).

Table 3: Comparison of propeller characteristics obtained with CFD and experiments for KCD-193 Propeller

	Experiment			***CFD***		
	K_T	$10K_Q$	η_0	K_T	$10K_Q$	η_0
Case 1	0.3739	0.5411	0.4138	0.36	0.5431	0.4149
Case 2	0.3707	0.554	0.4004	0.3631	0.5603	0.4053

Difference (%)		
	Case 1	*Case 2*
K_T	3.86	2.08
$10K_Q$	0.36	1.11
η	0.25	1.20

The CFD predictions for the performance characteristics of KCD-193 propeller in particular cavitating conditions are very close to that of experimental results given in Table 3.

5.2 Comparison of the Erosion Intensity Results

The implemented erosive indicators are compared against soft paint erosion experiments in this section. Illustration of the computed erosive intensity results for two cases are shown in the figures in this section followed by the corresponding propeller blade photo from the erosion experiments.

5.2.1 Case 1 results

Erosive intensity predictions of the Case 1 by IFM, GLM and Erosive Power Method (EPM) are shown below.

These functions are applied to flow solver as a field function and calculated separately for each conditions. After that, scalar scenes are created to investigate the erosion zones on the propeller blades.

In order to make meaningful predictions, the maximum and minimum scalar values of the erosive intensity is limited with threshold. The threshold is chosen as $-1*10^{-7}$ and $1*10^{7}$. It is determined by the maximum and minimum values of the calculated IFM, GLM and EPM values.

Generating the erosion intensity prediction figures in scalar scenes, blue-red colour map option is activated and opacity is taken as 1.0. This means the colours going to red and blue (max and min values of the thresholds) are showing the area of high erosion risk. Green colour, which represents '0' shows no erosion risk area.

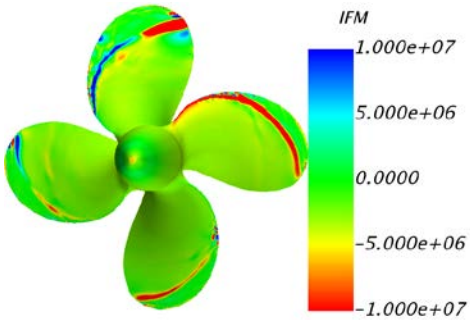

Figure 17: Erosion zones predicted by IFM

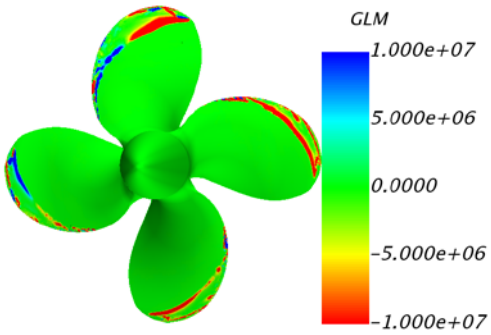

Figure 18: Erosion zones predicted by GLM

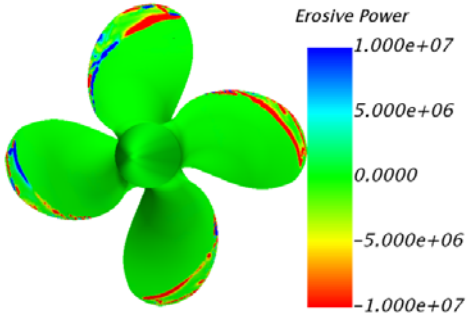

Figure 19: Erosion zones predicted by EPM

Erosion predictions for top right blade are shown below. They are at the same conditions with the erosive intensity figures for case 1 above. The only differences between the Figure 20 and Figures 17-19 are just colour (casting colour map is chosen) and opacity of the surface (taken as 0.75 instead of 1.0).

Blue colour shows high erosion risk area, red and yellow colour shows lower erosion risk area while bronze colour shows no erosion risk area in Figure 20.

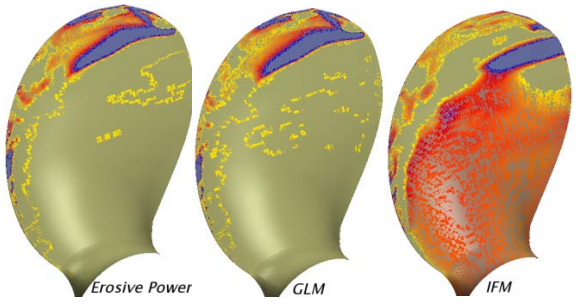

Figure 20: Comparison of erosion zones predicted by EPM, GLM and IFM erosive indicators.

Comparison between the erosion result from cavitation test and EPM prediction, when the position is at the Top Dead Centre (TDC), is shown below.

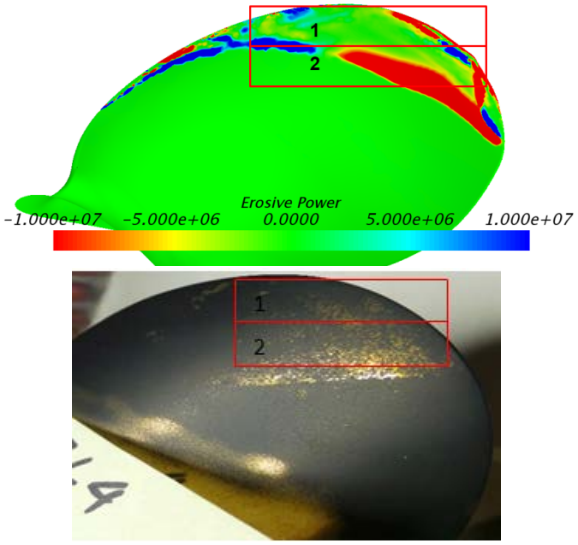

Figure 21: Comparison of erosion result from cavitation test and EPM

Cavitation erosion result from cavitation test and new proposed erosive power method illustrations show good agreement as can be seen from the figures.

5.2.2 Case 2 results

Erosive Intensity predictions of the Case 2 by IFM, GLM and new proposed Erosive Power Method are shown below.

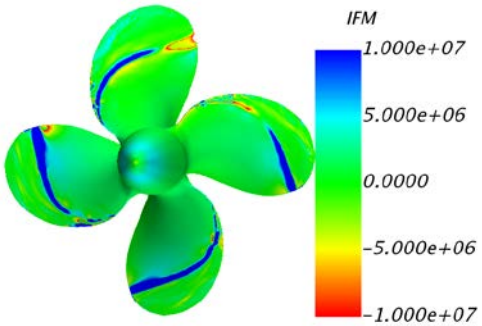

Figure 22: Erosion zones predicted by IFM

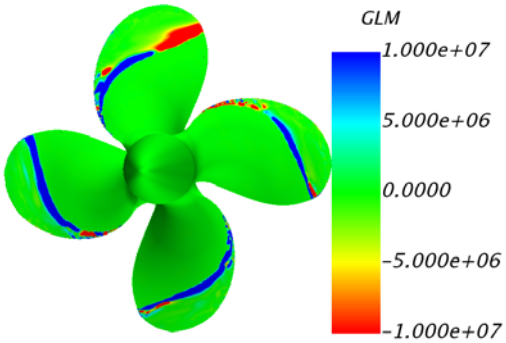

Figure 23: Erosion zones predicted by GLM

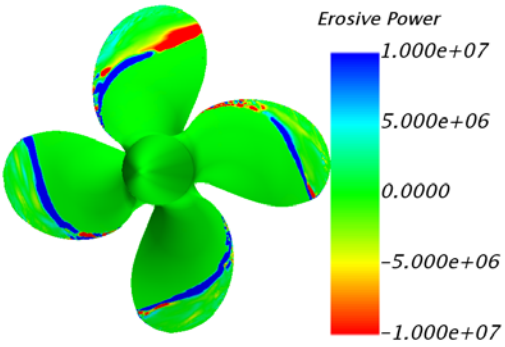

Figure 24: Erosion zones predicted by EPM

The colours going to red and blue (max and min values of the thresholds) are showing the area of high erosion risk. Green colour, which represents '0' represents no erosion risk area.

Erosion predictions for top right blade is shown in Figure 25 below.

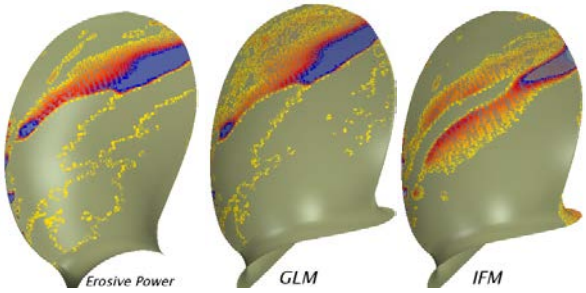

Figure 25: Comparison of erosion zones predicted by EPM, GLM and IFM erosive indicators

Comparison between the erosion result from cavitation test and EPM prediction, when the position is at the Top Dead Centre (TDC), is shown below.

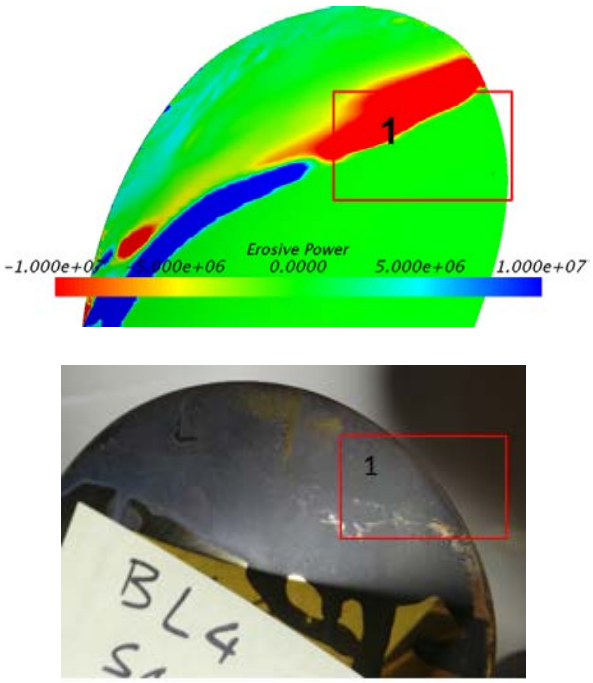

Figure 26: Comparison of erosion result from cavitation test and EPM

It should be mentioned that the erosion result presented in Figure 21 and 26 were observed after 30 min test in the cavitation tunnel. Undoubtedly, a CFD simulation of the full duration of the test would not be practical, as it could take too long to compute. In the current study after the analysis converged, it is assumed that damage on the propeller surface is time independent.

The estimation of the erosion intensity on propeller surface using erosive power method, the GLM and IFM do not need extra computational power and time as they are using already computed variables and can be regarded as without an additional computational cost.

It can be deduced from the figures that erosive indicators derived from computational simulations present significant similarities to the pitted soft paint pattern on the propeller blade observed after the erosion tests.

The pitting concentration for Case1, shown in the Figure 21, is composed of two main components. The region number 1 for this figure presents a pattern starts from the propeller tip and finishes at 0.7R as is progresses towards the trailing edge. Region number 2 in the same figure, starts from the mid-chord region of 0.7R and continues toward the trailing edge following the same radii. Both of these features may be attributed to the cavitation pattern observed in Figure 14. The propeller, in the sequence of figures present both bursting of tip vortex cavitation at the propeller tip and shedding of sheet cavitation from 0.7R. The occurrence of these phenomenon caused the forming of the pitting patterns on the propeller blade. Both of these features are captured successfully by GLM and erosive power methods as shown in Figure 18 and 19. IFM method, on the other hand still captures the pittings in region 2, however does not present as many similarities as other two methods for the region 1.

The erosion test results for Case 2 presents one region with extensive pitting formation. This is mainly due to the continuous attached cavitation formation for this low cavitation number condition as can be observed in Figure 16. These results in limited cavitation shedding formation concentrated to the border of thick sheet cavitation located in the trailing edge region of 0.7R. Whilst all three erosive indicators capture this finding successfully, IFM method seems to present better resemblance. The gold colour present for IFM method predictions occurring both for the blade in the wake shadow region and the one after the wake shadow are clear indicators.

Overall, carried out CFD simulations and implemented erosive indicators has shown to successfully replicate the cavitation erosion test results. Whilst, all three erosive indicators showed reasonable success, the proposed new erosive power method is excelled in both cases proving its potential.

6 CONCLUSIONS

A study of cavitating flow analysis on KCD-193 propeller and evaluation of erosive indicators is conducted using cavitation erosion experiment results.

Based on foregoing analysis it is concluded that

- Commercial CFD code, STAR-CCM+ can be used to solve advanced fluid flow phenomena like cavitation on marine propellers.
- For studying the details of a cavitating flow field, DES has a good potential to become a useful and reliable tool.
- New proposed Erosive Power Method (EPM), GLM and IFM can be used to predict erosive intensity on the propeller blade in cavitating flow conditions. However, specifying the user-given threshold on cavitation erosion predictions has a large influence on the accuracy of the calculations.
- A new erosive indicator is proposed based on a combination of pressure, cavitation volume, and the time derivatives of pressure and cavitation volume. Such an approach enabled this new method to capture erosion that may originate both/ due to pressure and/or cavitation volume variation.
- Furthermore, this study is an ongoing research and highlights the need for further work in the area of determining the erosion intensity thresholds numerically.

ACKNOWLEDGEMENTS

The current work is supported by TUBITAK 2214-A International Doctoral Research Fellowship Programme, Grant No. B.14.2.TBT.0.06.01-21514107-020-155998. The simulations are performed at the University of Strathclyde Glasgow, using High-Performance Computing for the West of Scotland (ARCHIE-WeSt) and at the School of Marine Science and Technology of the University of Newcastle. These supports are gratefully acknowledged by the authors. The authors also thank to Mr. Patrick Fitzsimmons, for his invaluable support, guidance and mentoring.

REFERENCES

Aktas, B., Atlar, M., Fitzsimmons, P., Shi, W., Turkmen, S., Sasaki, N. (2015). Systematic cavitation tunnel tests for cavitation noise prediction of commercial ships using a standard series approach, The 4th International Conference on Advance Model Measurement Technologies for the Maritime Industry, AMT 2015, Istanbul.

Ashton, N., Revell, A., Skillen, A., Poletto, R., Billard, F. & Laurence, D. (2014). Progress in Tools for Turbulence Modeling and Simulation, The University of Manchester & CD-adapco.

Atlar M. (2011). Recent upgrading of marine testing facilities at Newcastle University, 2nd International conference on advanced model measurement technology for the EU maritime industry, Newcastle upon Tyne.

Benjamin T. B. & Ellis A.T. (1996). The collapse of cavitation bubbles and the pressures thereby produced against solid boundaries, Phil. Trans. R. Soc. Lond. A, 260, pp. 221- 240.

Bergeles, G., Koukouvinis, P. K., Gavaises, M., Li, J. & Wang, L. (2015). An Erosion Aggressiveness Index (EAI) Based on Pressure Load Estimation Due to Bubble Collapse in Cavitating Flows Within the RANS Solvers, SAE International Journal of Engines, 8(5), pp. 2276-2284.

Bensow, R. E., Bark, G. (2010). Implicit LES Predictions of the Cavitating Flow on a Propeller, Journal of Fluids Engineering, Vol. 132, 041302, 1-10.

Bark, G., and Bensow, R. E. (2013). "Hydrodynamic Mechanisms Controlling Cavitation Erosion," Int. Shipbuild. Prog., 60(1), pp. 345–374.

Boorsma A., & Whitworth, S. (2011). Understanding Details of Cavitation, Second International Symposium on Marine Propulsors smp'11, Hamburg, Germany.

Chen, Y. L., and Israelachvili, J. (1991). New Mechanism of Cavitation Damage, Science, 252(5009), pp. 1157–1160.

Dular M. & Coutier-Delgosha O. (2009). Numerical Modelling of cavitation Erosion, Int. J. of Numerical Methods in Fluids.

Eskilsson, C., Bensow, R. E. (2015). Estimation of Cavitation Erosion Intensity Using CFD: Numerical Comparison of Three Different Methods, Fourth International Symposium on Marine Propulsors, smp'15, Austin, Texas, USA.

Fortes-Patella, R., Reboud, J.L., Briancon-Marjollet, L. (2004). A phenomenological and numerical model for scaling the flow aggressiveness in cavitation erosion, Workshop on Cavitation Erosion, Bassin d'essais des carenes,Val de Reuil, France.

Fortes-Patella, R., Challier, G., Reboud, J. L., and Archer, A. (2013). Energy Balance in Cavitation Erosion: From Bubble Collapse to Indentation of Material Surface, ASME J. Fluids Eng., 135(1), p. 011303.

Franc, J.P. & Michel J.M. (2004). Fundamentals of Cavitation: Springer.

Hasuike, N., Yamasaki, S., Ando, J. (2009). Numerical study on cavitation erosion risk of marine propellers operating in wake flow, Proceedings of the 7th International Symposium on Cavitation, CAV2009, Ann Arbor, Michigan, USA.

Hidalgo, V., Luo, X., Escaler, X., Huang, R. and Valencia, E. (2015). Numerical simulation of cavitation erosion on a NACA0015 hydrofoil based on bubble collapse strength, 9th International Symposium on Cavitation (CAV2015), Journal of Physics: Conference Series, **656** (2015) 012050.

Jian, W., Petkovsek, M., Houlin, M., Sirok, B., Dular, M. (2015). Combined Numerical and Experimental Investigation of the Cavitation Erosion Process, Journal of Fluids Engineering, Vol. 137 / 051302 pp. 1-9.

Iwai Y., Okada T.& Tanaka S. (1989). A Study of cavitation bubble collapse pressure and erosion, part2: Estimation of erosion from the distribution of bubble collapse pressures, Wear, Vol. 133, 233-243.

Koukouvinis, P.K., Bergeles, G., Gavaises M. (2015). A New Methodology For Estimating Cavitation Erosion: Application On A High Speed Cavıtatıon Test Rig, 6th European Conference on Computational Fluid Dynamics (ECFD VI).

Maasch, M., Turan, O., Khorasanchi, M., (2015), Unsteady RANSE and detached eddy simulations of cavitating flow, International Conference on Shipping in Changing Climates, Glasgow, United Kingdom.

Mantzaris, A., Aktas, B., Fitsimmons, P., Atlar M. (2015). Establishment and verification of reproducible method for coating propeller blades for erosive cavitation detection, The 4th International Conference on Advance Model Measurement Technologies for the Maritime Industry, AMT 2015, Istanbul.

Muscari, R., Mascio, A. D. & Verzicco, R. (2012). Modeling of vortex dynamics in the wake of a marine propeller. Elsevier Ltd, Computers & Fluids, 73, 15.

Nohmi, M., Iga, Y., Ikohagi, Y. (2008). Numerical prediction method of cavitation erosion. In: Conference proceeding on turbomachinery society of Japan, vol 59, pp. 49-54.

Ochiai, N., Iga, Y., Nohmi, M., and Ikohagi, T. (2012). "Study of Quantitative Numerical Prediction of Cavitation Erosion in Cavitating Flow," ASME J. Fluids Eng., 135(1), pp. 011302.

Petkovsek, M. and Dular, M. (2013). Simultaneous observation of cavitation structures and cavitation erosion, Wear, Vol. 300, pp. 55–64.

Ponkratov, D., & Caldas, A. (2015). Prediction of Cavitation Erosion by Detached Eddy Simulation (DES) and its Validation against Model and Ship Scale Results, Fourth International Symposium on Marine Propulsors, SMP'15, Austin, Texas, USA.

Rayleigh, L. (1917). On the pressure developed in a liquid during the collapse of a spherical cavity, Phil. Mag., 34.

Reboud, J. L., Stutz, B., and Coutier-Delgosha, O., 1998, Two Phase Flow Structure of Cavitation Experiment and Modeling of Unsteady Effects, Proc. 3rd Int. Sym. Cavitation, Grenoble, France.

Schnerr, G. H. & Sauer, J. (2001). Physical and Numerical Modeling of Unsteady Cavitation Dynamics. 4th International Conference on Multiphase Flow, New Orleans, USA.

Terwisga, T. J. C., Fitzsimmons, P., Li, Z., Foeth, E. J. (2009). Cavitation Erosion – A review of physical mechanisms and erosion risk models, Proceedings of the 7th International Symposium on Cavitation, Ann Arbour, Michigan, USA, CAV2009 – Paper No. 41.

Tseng, C. C. (2010). Modeling of turbulent cavitating flows, The University of Michigan, Department of Mechanical Engineering, Ph. D. Thesis,

Vallier, A. (2013). Simulations of cavitation – from the large vapor structures to the small bubble dynamics, Ph. D. Thesis, Department of Energy Sciences, Faculty of Engineering, Lund University.

Wang, Y. C., and Brennen, C. E. (1994). Shock Wave Development in the Collapse of a Cloud of Bubbles, ASME Paper No. FED Vol. 194, pp. 15–19.

Zhang, L., Zhang, N., Peng, X., Wang, B., Shao, X. (2015). A review of studies of mechanism and prediction of tip vortex cavitation inception, Journal of Hydrodynamics, vol. 27(4), pp. 488-495.

Li, Z. (2012). Assessment of Cavitation Erosion with a Multiphase Reynolds-Averaged Navier-Stokes Method, Delft University of Technology, Ph.D. Thesis.

Zwart, P. J., Gerber, A. G. and Belamri T. (2004), A Two-Phase Flow Model for Predicting Cavitation Dynamics". In Fifth International Conference on, Multiphase Flow, Yokohama, Japan.

DISCUSSION

We would like to thank to Drs. Papoulias, van Terwisga, Schenke and Helma for their interest in our work and insightful comments, questions and suggestions.

1. Discusser: Dimitrios Papoulias

Discusser e-mail: dimitrios.papoulias@cd-adapco.com

Comments from Dr. Papoulias

Cavitation erosion functions need to be time averaged over the simulation period.

$\frac{dp}{dt}$ will capture the pressure oscillations of the flow. We know that erosion related to the bubble pressure upon the collapse phase.

Authors' Closure

Thank you for your comment and your suggestion. We certainly agree that cavitation erosion is a time dependent phenomenon and we do plan to run our CFD simulations using the time averaged cavitation erosion functions. Unfortunately, these results have not been available in time for this paper.

As $\partial p/\partial t$ captures the pressure oscillations of the flow and we are studying on generating a new erosion intensity function that represents both pressure oscillations and bubble collapse. Also we are studying on how to add more information to the IFM.

2. Discusser: Tom van Terwisga

Discusser e-mail: t.v.terwisga@marin.nl

Comment and question from Dr. Tom van Tervisga

Comment: Li et al. (IFM) also stated to have the complete the relation for $\frac{dE_{pot}}{dt} = (\Delta P)\left(\frac{dV_v}{dt}\right) + V_{cav}\left(\frac{dP}{dt}\right)$ but why the $\frac{dP}{dt}$ term appeared most important in her case.

Question: Your EPM values show extreme $+(blue)$ and $-(red)$ values. But it is only after collapsing value (either + or -) that leads to erosion. Is this a correct interpretation?

Authors' Closure

Thank you for your comment and nice question. Yes, also in our simulations the pressure term, $\frac{dP}{dt}$ which captures pressure oscillations of the flow has very important role in the EPM results.

Erosive indicator values are instant results of the EPM equation as:

$$I_{EPM} = (P - P_v)\left(\frac{dV_v}{dt}\right) + V_V\left(\frac{dP}{dt}\right)$$

We have been studying how to interpret and implement the maximum (blue) and minimum (red) values of the erosive intensity results of our EPM values.

3. Discusser: Sören Schenke

Discusser e-mail: s.schenke@tudelft.nl

Questions from Mr. Schenke

What is the explanation for different erosive patterns at different blade positions in this case?

Was the erosive indicator calculated as an accumulation of individual events?

$I = \sum_i I_i$ (s. Li, Tervisga)

Authors' Closure

Thank you for your questions. Erosive patterns vary with blade positions. This is due to the non-uniform inflow introduced by the wake screen. The wake screen aids in recreating the axial inflow to the propeller in the presence of a ship hull in front of the propeller. The presence of the hull generates a wake shadow at the top dead center, which incorporates local slowed down flow velocity. Inherently this area experiences significant cavitation volume fluctuations. Therefore, the erosive patterns are not uniform and changes with the blade position.

No, erosive indicator was showing instant erosive intensities on the propeller blades. We have been studying on how to imply time averaged erosion indicator over the simulation period.

4. Discusser: Stephen Helma

Discusser e-mail: sh@smpropulsion.com

Question from Dr. Stephen Helma

Can you please explain the similarity of the results of CFD + paint test in the two cases presented?

Authors' Closure

Thank you for your question about the comparison of the CFD results with the experimental ones. The CFD simulations and implemented erosive indicators have shown to successfully predict the paint test results. Whilst, all three erosive indicators showed reasonable success, the proposed new erosive power method is excelled in both cases proving its potential.

The pitting concentration for Case1, shown in the Figure 21, is composed of two main components. The region number 1 in this figure presents a pattern from the propeller tip and to 0.7R position, which progresses towards the trailing edge. For the region number 2 in the same figure, the pattern starts from the mid-chord region of 0.7R and continues toward the trailing edge following the same radii. Both patterns may be attributed to the cavitation pattern observed in Figure 14. The propeller, in the sequence of figures present both bursting of tip vortex cavitation at the propeller tip and shedding of sheet cavitation from 0.7R. The occurrence of these phenomenon caused the forming of the pitting patterns on the propeller blade.

The erosion test results for Case 2 presents one region with extensive pitting formation. This is mainly due to the continuous attached cavitation formation for this low cavitation number condition as can be observed in Figure 16. These results in limited cavitation shedding formation concentrated to the border of thick sheet cavitation located in the trailing edge region of 0.7R.